Available online at www.sciencedirect.com

SCIENCE DIRECT®

Earth and Planetary Science Letters 234 (2005) 39–57

EPSL

www.elsevier.com/locate/epsl

Melt–peridotite interactions: Links between garnet pyroxenite and high-Mg# signature of continental crust

Yongsheng Liu[a,b,*], Shan Gao[a,b], Cin-Ty Aeolus Lee[c], Shenghong Hu[a], Xiaoming Liu[b], Honglin Yuan[b]

[a]*National Key Laboratory of Geological Processes and Mineral Resources, Faculty of Earth Sciences, China University of Geosciences, Wuhan 430074, China*

[b]*Key Laboratory of Continental Dynamics, Department of Geology, Northwest University, Xi'an 710069, China*

[c]*Department of Earth Science, MS-126, Rice University, Houston, TX 77005, USA*

Received 7 September 2004; received in revised form 15 February 2005; accepted 19 February 2005
Available online 19 April 2005
Editor: R.D. van der Hilst

Abstract

Abundant lherzolite, garnet pyroxenite and granulite xenoliths are found in the Neogene Hannuoba basalt of the North China craton. Garnet pyroxenites generally occur as veins/layers in spinel lherzolites. There is a gradual decrease in olivine and an increase in orthopyroxene mode going from the lherzolite to the pyroxenite, suggesting that orthopyroxene may be forming at the expense of olivine. Garnet pyroxenites are enriched in the highly incompatible elements (e.g., Rb, K, Na, Sr, Ba, Nb and Ta) but have high and uniform Ni contents and Mg#s (83–90). This set of geochemical observations is paradoxical because the enrichments in highly incompatible elements signify derivation from a melt having either an evolved character or a significant fluid component, but the high Ni contents and high Mg#s suggest a much more primitive origin. A somewhat similar paradox is observed in the granulite xenoliths. Many of the granulite xenoliths have intermediate compositions, characterized by $SiO_2 > 50$ wt.%, high Al_2O_3, Na_2O, and Sr contents, low Y and heavy rare-earth contents, and high Sr/Y, La/Yb and Na_2O/K_2O ratios. However, these intermediate granulites have unusually high Mg#s (54–71) and high Ni (21–147 ppm) contents for their SiO_2 contents and would otherwise suggest that these granulites are more primitive than their SiO_2 contents indicate.

It has been hypothesized that continuous melt–rock reaction between a silicic melt and ultramafic country rock (lherzolite) can convert olivine to orthopyroxene, ultimately resulting in the formation of a high Mg# garnet pyroxenite, similar to what is seen in the Hannuoba garnet pyroxenite composite xenoliths. In addition, silicic melts that have reacted with mantle peridotite would be predicted to have anomalously high Mg#s and Ni contents (due to the strong buffering capacity of peridotite for Mg and Ni), producing melts having compositions similar to the intermediate–mafic granulite xenoliths in this study. It is thus possible that the Hannuoba garnet pyroxenites and intermediate–mafic granulites share a common petrogenetic origin. Such a link is further supported by the fact that the rare-earth element abundance patterns of melts calculated to be in equilibrium with the garnet pyroxenites roughly coincide with that of the intermediate granulites. It is concluded that the Hannuoba garnet

* Corresponding author. Faculty of Earth Sciences, China University of Geosciences, Wuhan 430074, China. Tel.: +86 27 87483044/61361211.

E-mail addresses: yshliu@cug.edu.cn, yshliu@hotmail.com (Y. Liu).

0012-821X/$ - see front matter
doi:10.1016/j.epsl.2005.02.034

pyroxenite-bearing composite xenoliths may present the first physical evidence for the hypothesized melt–rock reaction necessary for generating evolved magmas with high Mg# and hence, high-Mg# andesitic signature of the continental crust.

Keywords: melt–peridotite interaction; garnet pyroxenite; high-Mg# granulite; North China

1. Introduction

The uppermost part of the Earth's mantle is tectonically active which renders it geochemically complex. Adiabatic decompression results in the generation of partial melts or fluids, which ascend to the Earth's surface to form oceanic crust and/or continental crust. Depending on what depth melt generation takes place, these melts/fluids must traverse part of the mantle before reaching the Earth's surface. Thus, while some parts of the uppermost mantle represent simple solid residues of partial melting, it is likely that other parts represent the end-products of metasomatic reactions between the mantle and various melts/fluids that have traversed the mantle. Studies of xenoliths and primitive mantle-derived magmas have shown that mantle metasomatism is ubiquitous [1–9]. If much of the mantle has been hybridized, an important question to ask is what role, if any, such hybridized mantle plays in the origin and evolution of the Earth's crust. It has been suggested that partial melting of hot subducting oceanic crust may have been an important process by which continental crust was generated in the Archean and Proterozoic [10–13]. This is based on observations of high Sr/Y ratios in Archean tonalite–trondjhemite–granodiorite (TTG) suites, which hint at the influence of a subduction component (high Sr) and the presence of large amounts of garnet during partial melting (low Y). The latter suggests a garnet-rich residue, such as eclogitized subducted crust (or other garnet pyroxenite lithologies). This hypothesis is supported by the fact that although high Sr/Y magmas (adakites) are rare in modem times, the places that they do occur are typically in regions where anomalously young (and hence hot) oceanic crust is being subducted and potentially melted [14,15]. The problem, however, is that the compositions of model average continental crust and adakitic magmas typically have Mg#s (100*Mg/(Mg+Fe), in atomic number) and Ni contents too high for either to have been derived from partial melting of an evolved source, such as eclogitized oceanic crust [16–18]. To resolve this issue, it has been hypothesized that the high Mg#s and Ni contents are due to reaction of silicic slab-derived melts with the peridotitic mantle wedge through which the melts traverse before reaching crustal levels [17].

Experimental studies indicate that the products of reaction between silicic slab melts and peridotite wallrock are likely to be garnet- and pyroxene-rich and have high Mg#s [19]. Although garnet pyroxenites occur in many xenolith suites (e.g., [20–23]), there is no clear consensus on their petrogenetic origins. Some garnet pyroxenites are likely to be high pressure cumulates [21], but others could clearly form by melt–rock reaction (e.g., [22]). Furthermore, the geochemical relationship between the reaction zones and the overlying continental crust has been obscured by additional metasomatic overprinting (e.g., the pyroxene-rich garnet peridotites found in cratonic environments [24]).

This study will look at details of the garnet pyroxenite veins found in peridotite xenoliths in Hannuoba, North China to investigate whether there are any links between the garnet pyroxenite veins and the high-Mg# intermediate–mafic granulite xenoliths. These garnet pyroxenites can be shown to be the products of silicic melt–peridotite reaction and not high pressure cumulates. Moreover, their trace-element compositions are in equilibrium with the overlying Mesozoic granulitic crust, which has trace-element compositions similar to modern adakitic magmas.

2. Geological setting and samples

2.1. Geological setting

The North China craton is one of the world's oldest cratons. The presence of $\geq$3.6 Ga crustal remnants exposed at the surface or in lower crustal xenoliths in

both the northern and southern parts of the block suggests that it has remained partially intact since the Early Archean [25,26]. Based on age, lithological assemblage, tectonic evolution and *P–T–t* paths, the North China craton can be divided into the Eastern Block, the Western Block and the intervening Trans-North China Orogen (insert of Fig. 1) [27]. The craton experienced widespread tectonothermal reactivation during the Late Mesozoic and Cenozoic as indicated by the emplacement of voluminous Late Mesozoic granites and extensive Tertiary alkali basalt volcanism. Based on petrological, geochemical and isotopic studies of some of the xenoliths entrained in these Tertiary basalts and Ordovician diamond-bearing kimberlites, the tectonothermal events may have resulted in replacement of the old, cold, thick and depleted lithospheric mantle by young, hot, thin and fertile lithospheric mantle resulting in lithospheric thinning [28–32] and lower crustal recycling [33]. The Hannuoba basalts occur along the northern margin of the Trans-North China Orogen and are dated at 14–27 Ma by the K-Ar method [34]. Abundant lower crustal and upper mantle xenoliths are found in these basalts. The xenoliths have been studied to varying extents [31,35–46]. The samples used in this study are summarized in Fig. 2 and described below.

2.2. Granulite xenoliths

Granulite xenoliths are dominantly mafic and intermediate with rare metasedimentary members. Based on geochronologic constraints, they were classified into three groups: ~ 160–120 Ma mafic–intermediate, ~ 1.8–2.0 Ga felsic and ~ 2.5 Ga intermediate granulites [44]. Combination of U–Pb zircon ages, Sr and Nd isotopes and trace-element compositions [37,41,44,46] suggests that the granulites have formed primarily in the Mesozoic, though a few may have formed in the Proterozoic and Archean. The Mesozoic granulites were interpreted as products of mantle-derived melt underplating [37,41,42,44], in which those with convex-upward REE patterns were

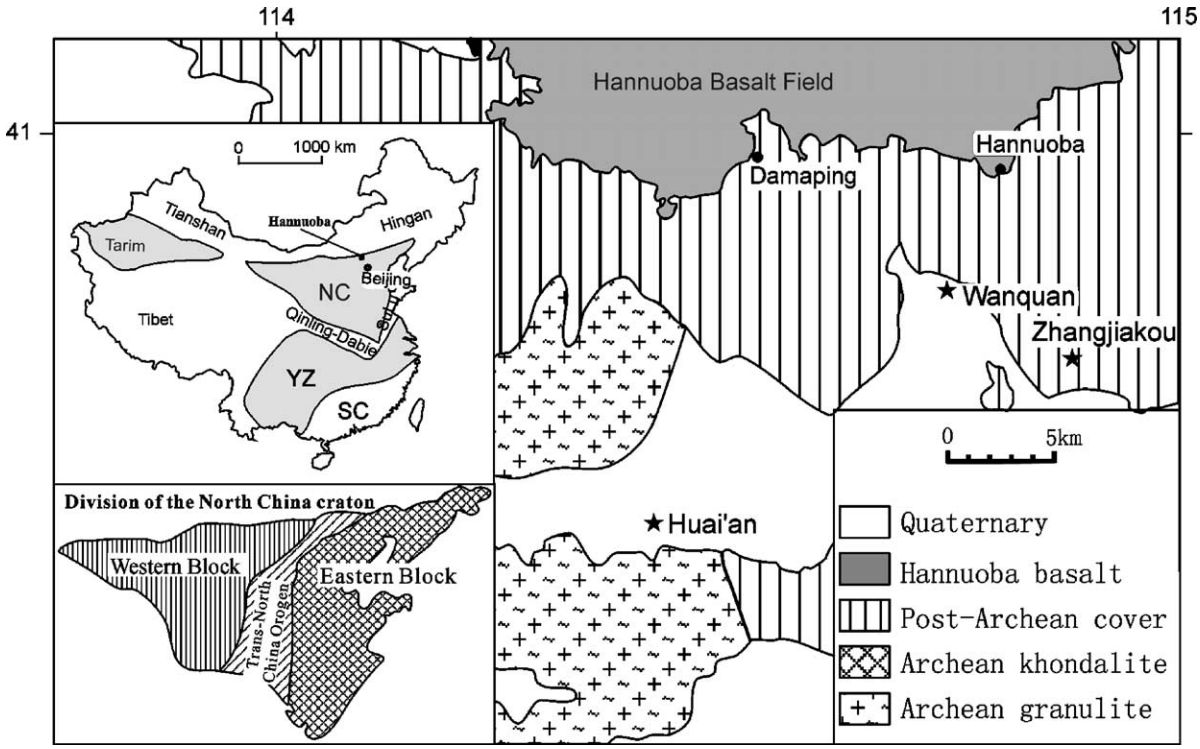

Fig. 1. Simplified geological map of the Hannuoba area. NC: North China craton, YC: Yangtze craton, SC: South China orogen. The division of the North China craton is after [27].

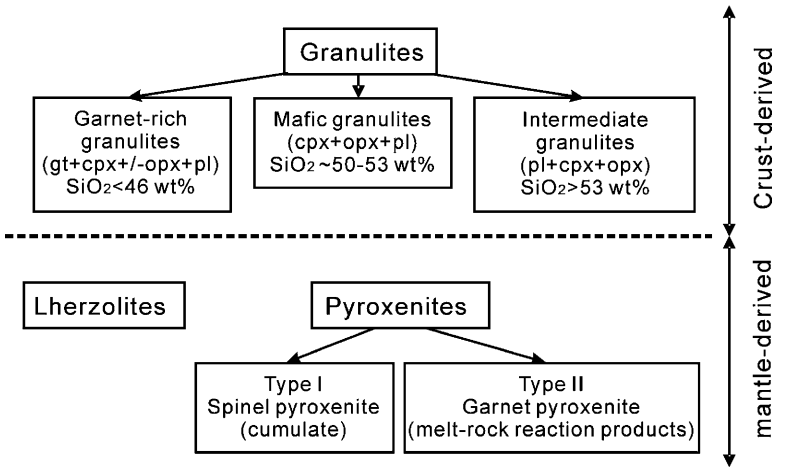

Fig. 2. Demographics for the samples used in this work.

pyroxene-dominated lower crustal cumulates [42]. In this work, we will focus on the Mesozoic granulites without obvious convex REE patterns, which have $SiO_2 > 50$ wt.%. Based on SiO_2 contents, they are classified as mafic granulites ($SiO_2 = 50–53$ wt.%) and intermediate granulites ($SiO_2 > 53$ wt.%) (Fig. 2).

Interestingly, all available geochemical data indicate that for a given SiO_2 content, the mafic and intermediate granulite xenoliths from Hannuoba tend to have high Mg#s, compared to the average worldwide granulite database and with granulite terranes exposed in the North China craton (Fig. 3). To illustrate, the Hannuoba granulite xenoliths plot on the high-Mg# end member of worldwide granulite xenoliths for $SiO_2 = 40–55$ wt.%. For $SiO_2 > 55–60$ wt.%, their Mg#s appear to plot above that of most samples in the worldwide database.

2.3. Peridotite and composite pyroxenite/peridotite xenoliths

The mantle xenoliths from Hannuoba are dominated by spinel lherzolites and pyroxenites. Pyroxenites were classified into garnet pyroxenites, garnet-free spinel pyroxenites and plagioclase-bearing pyroxenites based on the presence or absence of

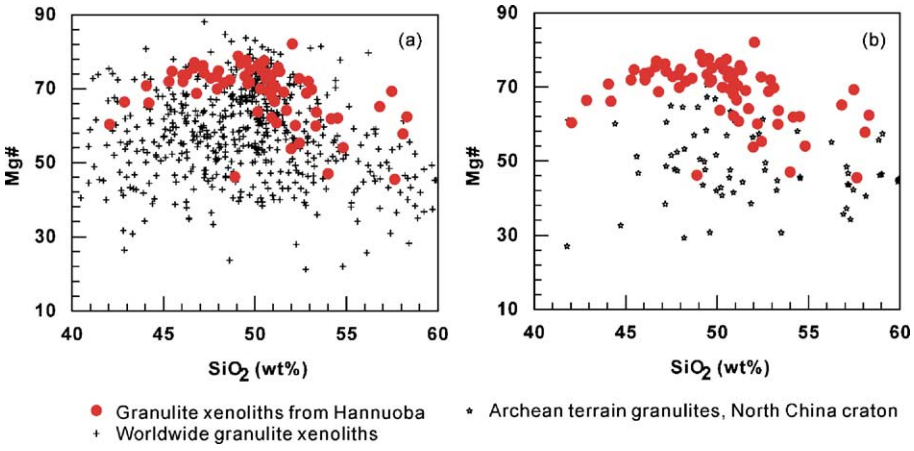

Fig. 3. Mg# vs. SiO_2 diagram of the Hannuoba granulite xenoliths with $SiO_2 = 40–62$ wt.% compared to worldwide granulite xenoliths (a) and Archean terrain granulites from the North China craton (b). Archean terrain granulite data from [69]. The Hannuoba granulite xenoliths include data of [40–42]. Worldwide granulite xenoliths data are from GERM (http://www.EarthRef.org).

aluminous phases such as garnet, spinel, and plagioclase. Two types of mantle-derived composite xenoliths were identified based on petrographic differences: clinopyroxene-rich spinel pyroxenite (cpx+ol+opx+sp) (type I) and garnet pyroxenite (opx+gt+cpx+ol+sp) (type II) veins hosted in spinel lherzolites (Figs. 2, 4a–c). These have previously been interpreted to be products of mantle metasomatism [35], high pressure cumulates [38,45] or subsolidus differentiates by modal segregation of different minerals within the upper mantle [39]. Certain petrologic and geochemical features of the composite xenoliths indicate that, at least some of the type II composite xenoliths are probably products of reaction between a silicate melt and peridotite.

Type I composite xenoliths are characterized by garnet-free pyroxenite layers hosted in lherzolite. The pyroxenite layer and lherzolite wall have the same mineral assemblages but different mineral proportions. The mineral proportions generally change sharply from the wall to the vein. For DMP-314, for example, major mineral proportions change from 75% ol, 15% opx, and 10% cpx in the lherzolite wall to 80% cpx, 15% opx, and 5% ol in the pyroxenite vein (Fig. 4a).

Type II composite xenoliths are characterized by garnet pyroxenite layers/veins hosted in spinel lherzolite (Fig. 4b and c). The spinel lherzolite is characterized by the following relative abundances of 50–70% ol, 25–5% cpx, 25–5% opx. Major mineral

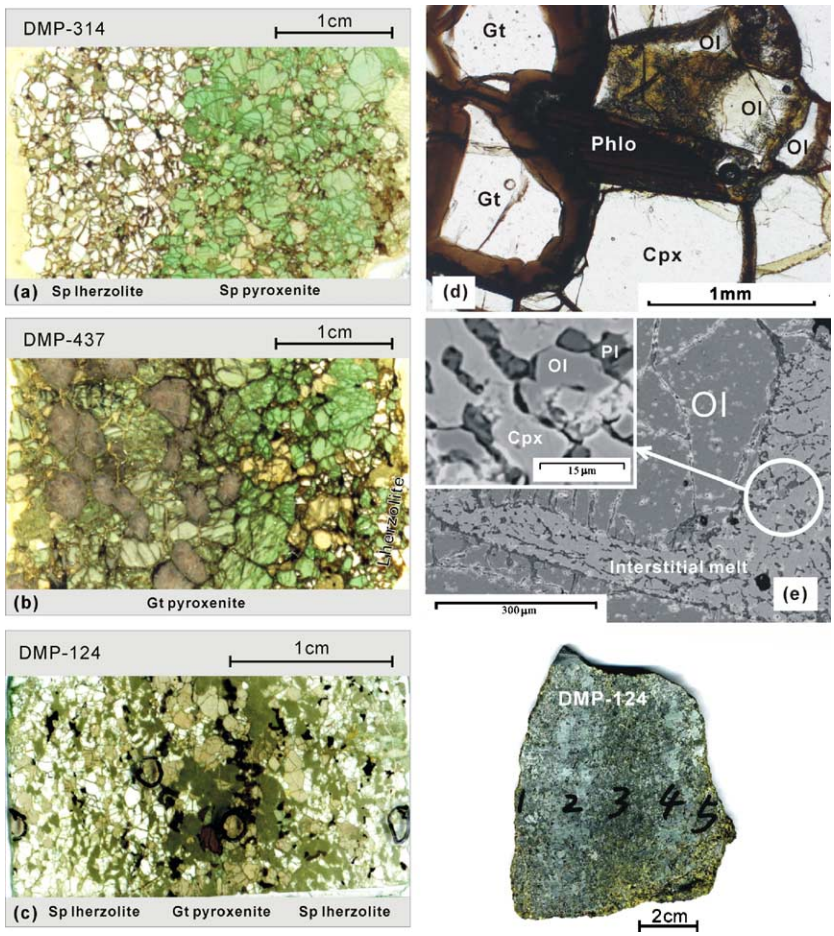

Fig. 4. (a, b) Thin section-scale pyroxenite veins in lherzolites; (c) sample DMP-124 and thin section-scale pyroxenite veins in lherzolites; (d) fresh garnet rimmed by kelyphite, and olivine (O1) was partially dissolved (JSB-01); (e) interstitial melt around olivine in DMP-124.

Table 1
Whole rock compositions

Sample	Type I				Type II							
	DMP-314 LW	DMP-314v PV	DMP-315 PV	DMP-407 PV	DMP-134 SPX	DMP-254 SPX	DMP-456 SPX	DMP-440 SPX	DMP-124 LW	DMP-124v PV	DMP-425 LW	DMP-425v PV
SiO_2	44.4	50.9	49.2	50.7	46.4	46.0					45.4	49.3
TiO_2	0.03	0.18	0.45	0.43	0.38	0.41					0.10	0.45
$A1_2O_3$	1.22	4.00	3.72	4.28	10.3	10.2					3.02	6.76
TFe_2O_3	9.24	5.20	8.86	12.9	6.68	7.04					8.33	4.44
MnO	0.13	0.11	0.14	0.17	0.14	0.15					0.12	0.10
MgO	44.2	26.8	20.4	24.6	21.1	23.2					38.8	19.4
CaO	0.63	9.97	15.4	6.12	11.7	10.8					2.62	15.0
Na_2O	0.05	0.57	0.38	0.27	0.59	0.71					0.18	0.97
K_2O	0.00	0.01	0.04	0.01	0.64	0.41					0.01	0.05
P_2O_5	0.01	0.01	0.01	0.01	0.06	0.05					0.01	0.03
LOI	0.52	0.74	1.04	0.85	1.69	0.93					1.08	1.57
Total	100	98.5	99.5	100	99.6	99.9					99.7	98.1
Na_2O/K_2O		57.0	9.50	27.0	0.92	1.73					18.0	19.4
Mg#	90.5	91.1	82.0	79.0	86.2	86.7					90.2	89.7
Sr/Y	5.90	7.70	7.30	10.1	13.7	14.2	32.8	11.4	8.89	7.38	3.80	4.50
Sc	9.43	27.5	59.2	32.5	30.5	90.2	27.1	27.8	8.84	13.3	11.1	41.6
V	34.3	184	196	166	264	302	166	212	66.9	124	67.7	257
Cr	2441	4961	2950	520	3003	2325	1730	1110	1658	2799	2461	4500
Co	145	78.2	91.3	127	92.2	104	58.7	93.4	98.3	70.7	125	61.2
Ni	2590	992	426	279	699	828	242	592	1781	1248	2080	652
Cu	138	103	176	58.0	142	76.2		46.6	35.1	88.5	80.8	143
Zn	110	79.8	125	80.5	88.2	29.1	0.82	27.5	90.5	94.3	96.6	92.9
Ga	2.04	3.87	7.36	8.28	11.1	8.71	5.22	11.9	4.56	6.61	3.74	6.06
Rb	0.67	0.92	0.89	0.90	16.2	10.8	11.8	8.57	2.76	3.90	1.06	2.22
Sr	5.30	41.0	70.9	71.2	219	245	500	256	27.9	48.8	9.15	64.3
Y	0.90	5.35	9.77	7.05	16.0	17.3	15.3	22.4	3.13	8.28	2.43	14.2
Nb	0.22	0.43	0.65	0.47	4.96	4.69	2.10	2.97	0.17	0.48	0.31	3.10
Cs	0.02	0.03	0.01	0.03	0.02	0.02	0.02	0.06	0.01	0.01	0.03	0.05
Ba	2.39	5.52	4.06	2.14	46.2	55.8	47.4	60.9	10.1	14.6	2.33	16.5
La	0.15	1.17	1.53	1.25	2.86	3.16	1.30	1.67	0.22	0.49	0.22	2.03
Ce	0.34	3.58	5.67	4.36	4.75	6.72	3.01	3.58	0.69	1.50	0.53	4.72
Pr	0.049	0.60	1.06	0.75	0.62	0.85	0.40	0.47	0.12	0.26	0.088	0.76
Nd	0.23	3.24	6.47	4.10	3.16	4.27	2.01	2.46	0.73	1.65	0.51	3.93
Sm	0.052	0.80	2.03	1.19	1.21	1.39	0.70	0.79	0.30	0.64	0.21	1.38
Eu	0.016	0.23	0.64	0.37	0.46	0.49	0.30	0.32	0.11	0.24	0.074	0.50
Gd	0.061	0.72	1.75	1.08	1.71	1.60	1.04	1.19	0.38	0.84	0.24	1.66
Tb	0.011	0.13	0.28	0.17	0.35	0.35	0.27	0.30	0.08	0.18	0.05	0.31
Dy	0.074	0.81	1.81	1.11	2.40	2.26	2.21	2.52	0.53	1.36	0.36	2.20
Ho	0.017	0.16	0.34	0.23	0.56	0.52	0.55	0.72	0.11	0.30	0.084	0.49
Er	0.050	0.53	0.96	0.64	1.57	1.43	1.75	2.30	0.31	0.86	0.23	1.37
Tm	0.009	0.082	0.14	0.10	0.24	0.21	0.30	0.41	0.05	0.14	0.043	0.21
Yb	0.050	0.48	0.75	0.60	1.41	1.33	1.87	2.57	0.27	0.84	0.24	1.29
Lu	0.008	0.071	0.11	0.085	0.21	0.20	0.29	0.40	0.04	0.13	0.034	0.19
Ta	0.07	0.06	0.05	0.06	0.30	0.36	0.20	0.25	0.01	0.03	0.07	0.19
Pb	2.28	2.07	3.09	0.81	2.31	0.76	0.77	0.85	1.55	1.68	1.87	2.77
Th	0.19	0.24	0.21	0.20	0.54	0.36	0.28	0.32	0.16	0.17	0.20	0.47
U	0.02	0.02	0.02	0.01	0.10	0.12	0.06	0.07	0.07	0.03	0.05	0.09
Zr	1.76	5.97	16.4	18.8	21.1	36.8	22.2	21.7	6.63	14.0	3.88	21.8
Hf	0.041	0.20	0.63	0.64	0.64	2.33	0.49	0.55	0.21	0.44	0.11	0.64

DMP-448 LW	DMP-448v PV	DMP-458 LW	DMP-458v PV	DMP-460 LW	DMP-460v PV	DMP-464 LW	DMP-464v PV	DMP-441 LW	DMP-441v PV	DMP-466 LW	DMP-466v PV	DMP-145 SPX
44.0	46.9	44.9	47.5	43.9	47.6	45.0	46.1	45.2	46.9	46.2	46.7	47.6
0.22	0.46	0.14	0.38	0.13	0.40	0.17	0.34	0.17	0.34	0.30	0.45	0.31
4.61	8.33	4.53	11.3	2.77	9.32	5.16	13.8	4.25	11.7	7.38	12.5	8.31
9.05	7.03	8.68	5.46	8.46	5.66	8.75	5.21	8.38	6.24	10.2	8.05	8.33
0.12	0.13	0.13	0.14	0.12	0.15	0.12	0.14	0.12	0.16	0.13	0.18	0.13
36.9	26.6	36.3	19.8	38.4	21.1	35.9	17.6	35.3	21.5	28.0	19.8	26.3
3.55	7.50	3.93	11.2	4.52	11.4	3.19	12.4	4.64	9.34	5.25	8.92	6.95
0.36	0.87	0.27	0.99	0.19	0.70	0.38	1.18	0.32	0.86	0.55	0.98	0.61
0.20	0.39	0.06	0.49	0.06	0.51	0.16	0.13	0.08	0.48	0.04	0.06	0.23
0.02	0.03	0.01	0.04	0.02	0.06	0.03	0.03	0.01	0.04	0.03	0.03	0.02
0.35	0.91	0.57	1.37	0.040	1.38	0.55	1.43	0.86	1.28	1.45	1.47	0.88
99.4	99.2	99.5	98.6	98.6	98.3	99.4	98.4	99.3	98.8	99.5	99.1	99.6
1.80	2.23	4.50	2.02	3.17	1.37	2.38	9.08	4.00	1.79	13.8	16.3	2.65
89.0	88.3	89.3	87.8	90.0	88.1	89.1	87.0	89.3	87.2	84.6	83.0	86.2
12.4	14.7	5.40	7.80	9.10	12.5	8.50	8.10	6.35	6.00	9.05	5.95	8.70
9.21	13.6	14.0	37.1	12.3	32.6	9.34	29.5	13.9	34.3	10.6	23.7	15.3
91.4	173	112	316	97.7	247	87.3	217	129	236	126	183	156
2403	2464	1793	1963	3137	2848	3126	1563	1891	1471	1863	1534	1985
156	118	133	113	145	96.2	152	107	190	104	113	81.8	93.6
1875	1313	1823	932	2292	705	1643	687	1865	822	1463	442	1075
67.7	180	124	179	219	126	102	192	99.1	129	109	45.6	127
93.1	105	105	117	112	35.2	99.3	124	54.6	87.7	93.7	20.3	98.4
5.28	7.98	4.95	9.57	4.15	7.48	5.88	11.4	4.38	6.83	9.23	8.50	8.30
4.73	8.69	1.91	16.0	1.76	12.2	2.80	2.83	3.13	13.9	1.53	2.09	5.79
61.9	194	25.0	195	18.7	213	24.6	111	37.7	174	44.6	119	80.0
5.01	13.2	4.65	25.1	2.06	17.0	2.89	13.7	5.94	29.0	4.93	20.0	9.20
0.84	1.89	0.32	2.72	1.58	5.27	1.81	2.05	0.30	2.47	0.57	0.68	0.52
0.01	0.02	0.01	0.03	0.01	0.02	0.01	0.01	0.02	0.02	0.01	0.01	0.02
23.2	43.5	7.94	71.0	6.88	104	11.9	36.7	11.9	56.9	4.30	9.14	24.0
0.70	1.62	0.28	1.92	0.94	3.17	1.09	1.48	0.29	1.71	0.35	0.61	0.95
1.97	4.38	0.84	4.84	1.67	5.90	2.18	3.53	0.96	4.10	1.15	1.95	2.36
0.31	0.63	0.14	0.73	0.21	0.74	0.27	0.47	0.17	0.57	0.19	0.34	0.32
1.70	3.68	0.82	3.66	1.03	3.68	1.24	2.58	0.99	2.93	1.20	2.01	1.82
0.55	1.16	0.34	1.23	0.37	1.16	0.35	0.85	0.35	1.00	0.48	0.90	0.66
0.18	0.42	0.13	0.47	0.12	0.43	0.12	0.37	0.16	0.40	0.21	0.40	0.25
0.61	1.42	0.48	1.83	0.41	1.55	0.41	1.17	0.61	1.64	0.67	1.40	0.81
0.12	0.26	0.10	0.38	0.068	0.32	0.072	0.24	0.12	0.40	0.13	0.34	0.18
0.77	1.98	0.72	3.20	0.37	2.48	0.44	1.88	0.85	3.42	0.81	2.84	1.32
0.16	0.45	0.15	0.79	0.067	0.62	0.092	0.44	0.19	0.91	0.17	0.70	0.33
0.45	1.33	0.46	2.56	0.13	1.79	0.24	1.29	0.52	3.03	0.41	2.16	0.97
0.074	0.21	0.07	0.44	0.021	0.32	0.038	0.24	0.09	0.56	0.063	0.38	0.18
0.40	1.35	0.41	2.89	0.11	2.08	0.24	1.44	0.50	3.52	0.30	2.52	1.02
0.055	0.21	0.057	0.43	0.014	0.32	0.031	0.23	0.073	0.57	0.038	0.36	0.17
0.16	0.20	0.086	0.26	0.14	0.42	0.22	0.24	0.16	0.26	0.073	0.099	0.10
1.70	2.28	2.22	2.42	2.62	1.29	1.87	2.62	1.34	1.95	2.34	0.87	1.95
0.24	0.30	0.20	0.35	0.28	0.60	0.30	0.36	0.18	0.33	0.19	0.21	0.18
0.04	0.06	0.01	0.06	0.05	0.16	0.06	0.14	0.01	0.06	0.09	0.06	0.03
12.7	25.1	7.32	28.3	6.57	25.2	9.63	19.2	7.71	26.5	11.9	25.4	14.0
0.37	0.71	0.19	0.73	0.20	0.79	0.24	0.48	0.22	0.62	0.33	0.69	0.43

(continued on next page)

Table 1 (*continued*)

Sample	Intermediate–mafic granulites					
	DMP-236	DMP-251	DMP-284	DMP-508	DMP-255	DMP-278
Ref.	This work					
SiO_2	54.5	53.3	53.4	53.2	51.2	50.2
TiO_2	0.46	0.72	0.51	0.92	0.59	0.51
$A1_2O_3$	19.1	18.1	19.2	16.9	16.1	11.3
TFe_2O_3	5.53	7.29	6.73	7.91	11.1	14.0
MnO	0.07	0.10	0.09	0.11	0.14	0.21
MgO	4.57	5.51	5.95	7.01	8.67	12.4
CaO	7.37	7.78	8.36	6.36	6.43	7.21
Na_2O	4.33	3.63	3.59	3.85	2.81	1.96
K_2O	1.75	1.81	1.38	1.67	1.29	0.63
P_2O_5	0.07	0.14	0.08	0.30	0.06	0.16
LOI	2.66	1.60	1.17	1.74	2.08	1.16
Total	100	100	100	100	98.4	98.5
Na_2O/K_2O	2.47	2.01	2.60	2.3 1	2.18	3.11
Mg#	62.1	60.0	63.7	63.8	60.8	63.7
Sr/Y	184	159	157	50.6	53.2	26.2
Sc	13.1	21.3	17.1	17.0	39.4	69.4
V	205	132	130	181	303	170
Cr	119	94.7	70.2	53.4	230	351
Co	40.1	27.6	67.9	23.4	47.4	82.4
Ni	63.5	37.5	100	21.4	147	91.6
Cu	47.3	11.1	11.3		54.1	9.61
Zn	50.8	72.8	57.4	86.0	82.4	146
Ga	18.1	18.3	16.1	22.3	15.3	17.0
Rb	27.3	23.3	20.0	11.7	33.9	18.9
Sr	1582	1345	1203	900	934	752
Y	8.58	8.46	7.69	17.8	17.5	28.8
Nb	3.81	1.33	1.74	5.35	2.88	2.57
Cs	0.07	0.03	0.02	0.05	0.09	0.09
Ba	508	960	728	776	338	273
La	4.41	11.1	8.88	21.7	4.55	14.1
Ce	9.18	21.8	18.2	47.9	10.9	35.9
Pr	1.13	2.62	2.13	5.87	1.57	4.93
Nd	5.33	11.8	9.40	26.4	8.09	22.7
Sm	1.26	2.19	1.77	5.22	2.13	4.93
Eu	1.23	1.33	1.11	1.67	1.10	1.31
Gd	1.22	1.96	1.54	4.48	2.04	4.21
Tb	0.20	0.26	0.23	0.62	0.38	0.71
Dy	1.14	1.31	1.18	3.22	2.22	3.91
Ho	0.26	0.27	0.24	0.58	0.51	0.86
Er	0.74	0.71	0.63	1.57	1.40	2.28
Tm	0.12	0.11	0.10	0.23	0.22	0.36
Yb	0.83	0.69	0.58	1.32	1.56	2.33
Lu	0.14	0.11	0.09	0.21	0.23	0.36
Ta	0.24	0.09	0.13	0.24	0.16	0.16
Pb	1.96	5.39	4.19	6.87	1.52	1.81
Th	0.23	0.04	0.16	0.20	0.30	0.15
U	0.24	0.03	0.10	0.02	0.18	0.09
Zr	28.9	36.0	40.0	100	47.6	71.6
Hf	0.77	0.98	1.59	2.58	0.99	2.15

LW=lherzolite wall; PV=pyroxenite vein/layer; SPX=single pyroxenite xenolith. Units are wt.% for major elements and ppm for trace elements.

					Lower crust
DMP-73	90DA5	91DAl	9lDA3	91SANl	
[42]	[40]				[48]
54.8	51.1	50.9	52.4	53.1	53.4
1.15	0.72	0.25	0.38	0.37	0.82
17.1	15.3	15.9	16.7	18.9	16.9
7.70	8.77	10.4	7.08	6.43	9.52
0.10	0.13	0.13	0.10	0.09	0.10
4.58	8.80	11.1	9.53	7.51	7.24
6.65	9.11	4.25	9.03	9.18	9.59
4.30	2.55	2.96	2.53	2.89	2.65
2.14	0.98	0.84	0.82	0.76	0.61
0.33	0.09	0.03	0.04	0.14	0.10
	1.82	3.82	0.84	1.20	
98.8	97.5	96.8	98.7	99.4	
2.01	2.60	3.52	3.09	3.80	4.33
54.1	66.5	68.0	72.7	69.8	60.2
68.5	105	475	218	260	21.8
21.3					31.0
140	204	95.0	95.0	83.0	196
73.8	121	120	130	85.0	215
22.4	40.0	45.0	30.0	21.0	38.0
31.9	58.0	190	109	71.0	88.0
14.9		150			26.0
114		110			78.0
22.0					13.0
27.1	19.0	22.0	13.0	20.0	11.0
1069	1000	960	1200	1170	348
15.6	9.50	2.02	5.50	4.50	16.0
9.91	2.00	1.33	1.95	1.83	5.00
0.08	0.06	0.70	0.03	0.01	0.30
1447	900	660	450	900	259
28.3	8.50	3.65	5.00	6.50	8.00
62.6	20.0	5.50	10.0	12.0	20.0
7.68	2.50	0.73	1.35	1.50	2.38
31.2	12.0	2.50	6.40	6.50	11.0
5.76	2.50	0.42	1.35	1.45	2.80
1.77	1.20	0.53	0.75	0.80	1.10
5.31	2.30	0.40	1.40	1.40	3.10
0.65	0.35	0.06	0.23	0.20	0.48
3.12	2.00	0.42	1.20	1.07	3.10
0.56	0.39	0.09	0.23	0.23	0.68
1.53	1.13	0.28	0.71	0.55	1.90
0.20	0.15	0.04	0.09	0.08	0.24
1.20	0.90	0.27	0.60	0.48	1.50
0.18	0.14	0.05	0.09	0.07	0.25
0.40	0.10	0.16	0.25	0.19	0.60
13.8	3.30	2.74	2.10	4.00	4.00
0.22	0.28	0.10	0.21	0.24	1.20
0.18	0.09	0.15	0.06	0.05	0.20
119	95.0	62.0	89.0	80.0	68.0
3.44	1.10	0.38	0.72	0.50	1.90

proportions of garnet pyroxenite veins vary significantly for different samples, 5–60% for garnet and orthopyroxene, 5–30% for clinopyroxene and 5–30% for olivine. Grain sizes in garnet-bearing composite xenoliths increase gradually from the wall (mostly <2 mm in diameter) and into the garnet pyroxenite vein (mostly 2~10 mm in diameter). Some xenoliths were collected as garnet pyroxenites without peridotite host rocks. These have similar mineral assemblage and structure (e.g., coarse grained) to garnet pyroxenite veins/layers. These could be fragments of thick garnet pyroxenite layers/veins. Although garnets in most samples have decomposed into kelyphite assemblages consisting of extremely fine-grained spinel and plagioclase, their bulk compositions still preserve the major element composition of pyrope-rich garnet as demonstrated by microprobe analysis using large beam sizes (7–10 μm) [43]. Fresh garnet cores with kelyphite rims are preserved in garnet pyroxenites DMP-457 and JSB-01 (Fig. 4d). Finally, some xenolith samples contain interstitial silicate glasses (Fig. 4d–e). These glasses may have formed as a result of heating, decompression, and/or infiltration of host melt during transport of xenoliths to the surface.

For the samples in this work, last equilibrium temperatures range from 980 to 1000 °C for spinel lherzolites [31], 950 to 1040 °C for garnet pyroxenites, 770 to 915 °C for garnet-bearing mafic granulites [43] and ~ 910 °C for garnet-free granulites [42]. Last equilibrium pressures vary from 10 to 18 kbar for garnet pyroxenites and 9–11 kbar for garnet bearing mafic granulites [43]. The geothermobarometry imply that the granulites and pyroxenites were spatially close in the lithospheric column.

3. Analytical methods

The xenoliths under investigation are <8 cm across. The pyroxenite vein and lherzolite/pyroxenite wall was separated by sawing and then washed and crushed to about 60 mesh in an alumina jaw crusher. About 60 g of the sample split was powdered in an agate ring mill to less than 200 mesh for whole rock analysis.

Whole rock major elements were analyzed by X-ray fluorescence spectrometry (Rikagu RIX 2100) at the Key Laboratory of Continental Dynamics, Northwest University, China. Analyses of a USGS basalt standard indicate precision and accuracy both better than 4% [31]. Trace element compositions are analyzed by ICP-MS at China University of Geosciences and Northwest University, China. Analytical procedure is the same as in [42]. Analyses of the international rock standards BHVO-1 and BCR-2 indicate that the analytical precision is mostly better than 5% as indicated by the relative standard deviation (RSD). Whole-rock compositions of the xenoliths are listed in Table 1. In-situ trace element analyses of clinopyroxene in Table 2 were performed by Laser-Ablation-Inductively Coupled Plasma Mass Spectrometry at the Key Laboratory of Continental

Table 2
Parameters used for melt calculations

	Partition coefficients				Concentrations (ppm)			
	[67]		[68]		DMP-124 (garnet-poor)		DMP-440 (garnet-rich)	
	gt	cpx	opx	ol	cpx	whole rock	cpx	whole rock
La	0.025	0.052	0.031	0.0028	1.14	0.49	0.76	1.67
Ce	0.04	0.105	0.0277	0.002	4.01	1.50	2.93	3.58
Nd	0.086	0.28	0.0279	0.0003	5.00	0.26	4.52	2.46
Sm	0.83	0.444	0.0278	0.0049	2.16	1.65	1.16	0.79
Eu	0.74	0.604	0.0276	0.0006	0.78	0.64	0.54	0.32
Gd	1.13	0.65	0.0388	0.0069	2.71	0.24	0.98	1.19
DY	4.4	0.78	0.0762	0.0095	3.06	0.84	1.23	2.52
Er	11	0.99	0.1526	0.0064	1.40	0.18	0.58	2.30
Yb	14	0.64	0.254	0.0313	0.84	1.36	0.45	2.57
Lu	16	0.79	0.323	0.0473	0.12	0.30	0.05	0.40

Dynamics, Northwest University. The laser-ablation system is a GeoLas 200M (MicroLas, Gottingen, Germany), which is equipped with a 193 nm ArF-excimer laser and a homogenizing, imaging optical system. The ICP-MS is an Elan 6100-DRC. External calibration was performed using NIST 610. Ca was used for internal standardization. Gao et al. [47] reported the analytical details and analysis of NIST SRM (610, 612, 614) and USGS (BCR-2G, BHVO-2G, BIR-1G) glasses.

4. Geochemical features

4.1. Type I spinel pyroxenites

Type I pyroxenites have low Al_2O_3, Na_2O, K_2O, Rb and Ba contents similar to the concentrations of these elements in peridotite (Figs. 5 and 6a–c). However, their Mg#s are highly variable, ranging from 79 to 91 compared to the narrow range seen in the peridotite xenoliths (89–91). The type I pyrox-

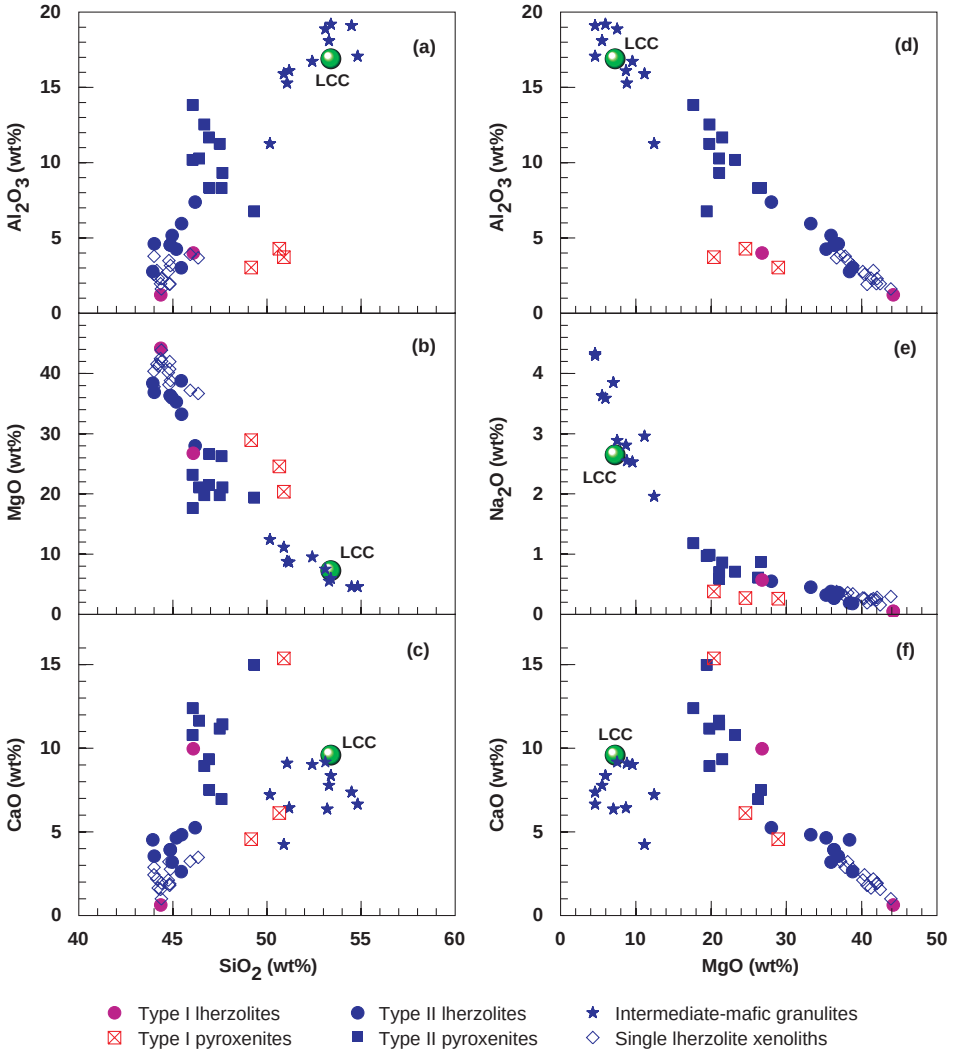

Fig. 5. Plots of SiO_2 and MgO vs. Al_2O_3, CaO and Na_2O. Single lherzolite xenoliths from [31]. Lherzolite wall of DMP-314 is thought to be high pressure cumulate. Literature data [40,42] for intermediate–mafic and granulites with SiO_2>50 wt.% and without convex-upward REE patterns are also included. Lower continental crust (LCC) estimates from [48].

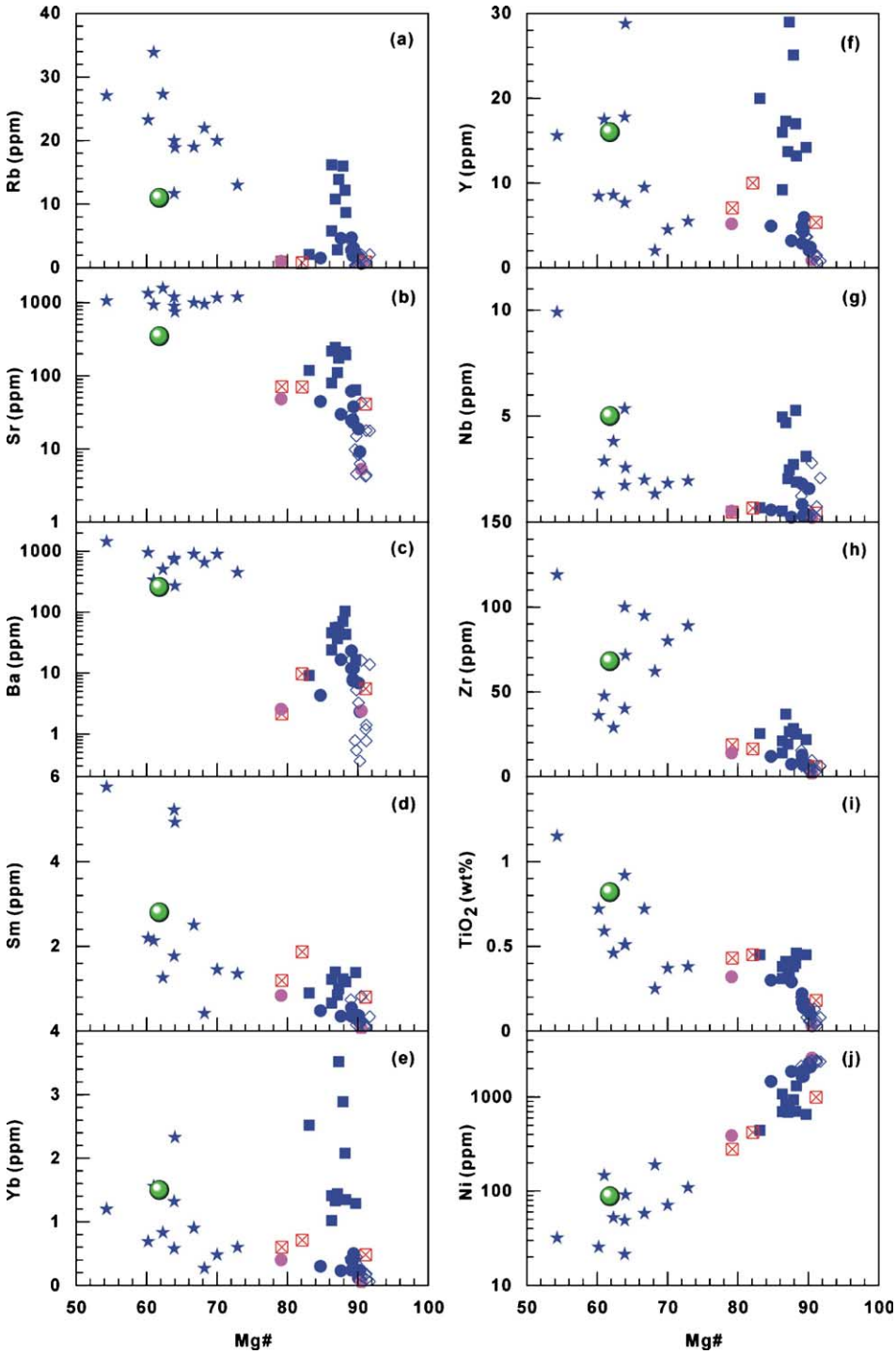

Fig. 6. Plots of Mg# vs. trace elements and TiO_2. Symbols as in Fig. 5.

enites also have significantly lower Ni contents than peridotite xenoliths (Fig. 6j) and show convex upwards rare earth elements (REE) patterns with slight enrichments in the LREE (Fig. 7b).

4.2. Type II garnet pyroxenites

Type II pyroxenites differ from the Type I pyroxenites in having significantly higher K_2O, Na_2O, Al_2O_3, Rb, Ba, and Sr contents (Figs. 5 and 6). These enrichments in large ion lithophile elements (K, Rb, Ba, and Sr) are characteristic of interaction with an evolved melt or fluid-bearing melt because these elements are highly incompatible and fluid-mobile. Paradoxically, however, their Mg#s range from 83 to 90, which are not only higher than most of the Type I pyroxenites but overlap with that of residual peridotites (Fig. 6). In addition, the Type II pyroxenites have higher Ni contents than most of the Type I pyroxenites. The Type II pyroxenites also have slightly greater concentrations of high field strength element (e.g., Nb, Ta, and Zr), HREEs and Y. The LREE-enriched character gives rise to generally concave REE abundance patterns, which differs from the convex patterns of the Type I pyroxenites (Fig. 7b and e). The HREE enrichments are consistent with the presence of garnet in the Type II pyroxenites. The Mg#s and Ni contents of the Type II garnet pyroxenites are significantly higher than the Hannuoba mafic granulite xenoliths, many of which are garnet- and pyroxene-rich [42]. These granulite xenoliths undoubtedly have a crustal origin indicated by their unradiogenic Nd ($\varepsilon_{Nd(0)}$ = − 12.6–19.3) and radiogenic Sr isotopic ($^{87}Sr/^{86}Sr$=0.707–0.709) compositions [44].

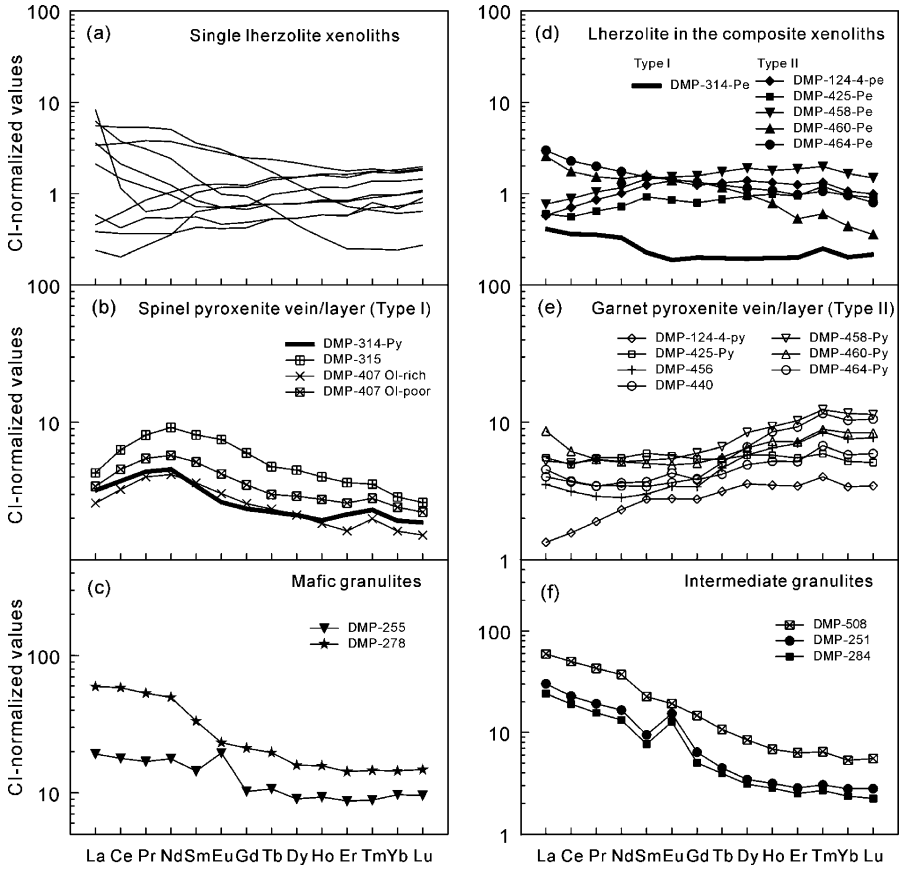

Fig. 7. Chondrite (CI)-normalized REE patterns. Single lherzolite xenoliths in (a) are from [31]. CI values are from [70].

4.3. Granulite xenoliths

The mafic and intermediate granulite xenoliths have relatively high Mg#s (54–71 with an average of 64) and Al_2O_3 (11.3–19.2 wt.%), Na_2O (2.0–3.9 wt.%) and Ni contents (21–147 ppm) (Table 1). For their SiO_2 contents (~ 50–55 wt.%), these Mg#s appear to be anomalously high given that mid-ocean ridge basalts (SiO_2 ~50 wt.%) have on average Mg#s of only 55. The Al_2O_3 contents and Mg#s are also higher than model estimates of the bulk continental crust, but they are very similar to model estimates of global low crustal compositions [48] (Figs. 5 and 6; Table 1). The granulite xenoliths are also characterized by high Sr contents (752–1582 ppm), and high Sr/Y (26–260), La/Yb (2.9–24) and Na_2O/K_2O (2.0–3.8) ratios (Table 1). They are characterized by flat and depleted HREE abundance patterns and by the presence or absence of positive Eu anomalies (Fig. 7c and f). Many of these features (e.g., high Sr/Y and flat HREE patterns) are similar to so-called adakitic lavas, which have been interpreted to represent silicic melts derived from partial melting of a garnet-bearing source, such as eclogitized subducted oceanic crust [19,49].

5. Discussion

5.1. The case for melt–peridotite interaction: transition from lherzolite to garnet pyroxenite

We now discuss the origins of the Type I and Type II pyroxenites. These pyroxenites differ fundamentally in several aspects. First, in terms of overall mineralogy and texture, the transition between the Type II garnet pyroxenite veins and the lherzolite wallrock is gradual. This contrasts with the very sharp transition between Type I spinel pyroxenite veins and the lherzolite wallrock (Fig. 4). Second, within the transition zone between Type II garnet pyroxenite and lherzolite, there is a gradual decrease in olivine and an increase in orthopyroxene mode going from the lherzolite to the pyroxenite (Fig. 4b–c). This suggests that orthopyroxene may be forming at the expense of olivine. Third, unlike lherzolites and Type I pyroxenites, the Type II garnet pyroxenites are enriched in the highly incompatible elements (Rb, K, Na, Sr, Ba, Nb and Ta) but have high and uniform Ni contents and Mg#s (83–90) (Figs. 5 and 6). This set of geochemical observations is paradoxical because the enrichments in highly incompatible elements signify derivation from a melt having either an evolved character or a significant fluid component, but the high Ni contents and high Mg#s suggest a much more primitive origin. These features suggest that the Ni content and Mg# of the pyroxenite veins was probably "buffered" during their formation [50]. In contrast, the Type I pyroxenites have lower and more variable Ni contents and Mg#s as well as highly incompatible elements (Rb, K, Na, Sr, Ba, Nb and Ta).

Various hypotheses have been put forward to explain the origin of these pyroxenites. These include formation by modal segregation [39], modal metasomatism/melt–rock reaction [35], and/or cumulate processes [38,45]. Modal segregation is unlikely for either type of pyroxenites. On the one hand, modal segregation alone cannot explain the enrichments in highly incompatible elements in the Type II garnet pyroxenites (Figs. 5–7). On the other hand, the Type I spinel pyroxenites show LREE-enriched and convex REE abundance patterns (Fig. 7b) and highly variable Mg# and Ni (Table 1), which are typical of clinopyroxene-rich cumulates derived from LREE-enriched basaltic magmas.

However, we interpret the above features to indicate that the Type II garnet pyroxenites represent melt–rock reaction between an evolved melt and peridotite, while the Type I pyroxenites probably represent cumulates from a fractionally crystallizing magma in a dike or magma chamber as suggested by Xu [45]. By melt–rock reaction, we specifically mean the continuous porous flow of melt through peridotite without significant net crystallization from the melt. A melt that is continuously reacting with the rock through which it passes will likely have its composition buffered, which may explain not only the high Ni contents and Mg#s in the Type II garnet pyroxenites but also their remarkable uniformity (Fig. 6j). Fractional crystallization, on the other hand, will cause the melt composition to evolve; this evolution will be manifested as variable compositions in the cumulates, possibly explaining the variable Ni contents and Mg#s of the Type I pyroxenites. Melt–rock reaction should also be manifested in terms of reaction zones as seen in the Type II garnet pyroxenites but not

in the Type I spinel pyroxenites, which display sharp wallrock–vein contacts.

Finally, we suggest that the melt responsible for forming the Type II garnet pyroxenites was probably silicic. Formation of orthopyroxene at the expense of olivine, as seen in our samples, is the reaction product predicted from phase petrology between a silicic melt and a lherzolite or harzburgite. This has been confirmed by recent experiments by Rapp et al. [19], who showed that reaction between peridotite and a silicic melt would result in the formation of garnet and orthopyroxene-rich reaction zones. It has also been shown that in such reactions, orthopyroxene mode can increase while Mg#s and Ni contents remain roughly buffered [24].

The question that now arises is what could be the source of a silicic melt within the mantle. It is probably not possible to generate a silicic melt by direct partial melting of peridotite [51–54]. However, melting of basaltic crust, either in the form of a subducting slab or delaminated lower crust, can generate a silicic melt [8,33,55,56]. There is yet no direct evidence for slab melting, but some magmas with high Sr/Y ratios (so-called adakites) have been interpreted to have formed by partial melting of an "eclogitic" source [14], such as subducted oceanic crust or delaminated continental lower crust (e.g., [18,57,58]). The problem is that such magmas have Ni contents and Mg#s too high to be simply direct melts of a basaltic protolith. Proponents of this hypothesis have suggested that slab-derived silicic melts must undoubtedly react with the mantle wedge through which they pass [17,59–61]. If the Type II garnet pyroxenites were indeed converted from lherzolite by melt–rock reaction, they may represent the first physical evidence for these hypothesized melt–rock reaction zones in the mantle.

5.2. Link between the garnet pyroxenites and intermediate–mafic granulites

As discussed above, the mafic and intermediate granulites are characterized by (1) anomalously high Mg#s for their SiO_2 contents, (2) high Sr/Y, Al_2O_3, and Na_2O values, and (3) depleted and flat HREE patterns. These characteristics are typical of so-called adakitic lavas, which have been hypothesized to originate by partial melting of eclogitized subducted oceanic crust followed by reaction with the overlying mantle through which the melt passes [17,19,59–61]. Reaction of the silicic melt with the mantle appears to be necessary because partial melts of eclogitized oceanic crust should have Mg#s (<45; [8,55,62,63]) less than that of typical oceanic crust (~ 55). Indeed, experimental studies have confirmed that reaction of a silicic melt with peridotite can yield evolved melts with high Mg# (>51; [19]) and accordingly, melt–rock reaction products with high and "buffered" Mg#s.

If the Type II garnet pyroxenites are interpreted to be reaction products between silicic melt and mantle peridotite, and the intermediate granulites are interpreted to be melts derived by such reactions, the question arises as to whether these two rock types in Hannuoba are in fact petrogenetically linked. Below, we list three lines of evidence that are consistent with such a link.

1) Assuming a K_D(Fe/Mg) for pyroxenes of ~ 0.3, the high Mg#s of the intermediate granulites (54–71) predict Mg#s of ~ 80–89 in the solids (e.g., the solid residues or cumulates) with which they were last in equilibrium. These predicted Mg#s are consistent with those of the Type II garnet pyroxenites (83–90).
2) The Ni contents of melts in equilibrium with the Type II garnet pyroxenites (440–1300 ppm) should be roughly in the range of 50 to 200 ppm, which overlaps the range seen in the mafic–intermediate granulites (20–150 ppm).
3) The REE abundance patterns of calculated melts in equilibrium with the Type II garnet pyroxenites coincide with that of the intermediate granulites. The liquid composition was calculated using both the trace element composition of the bulk rock and the trace element composition of the clinopyroxene, the latter determined by laser ablation ICP-MS. The partition coefficients used are given in Table 2. The single mineral approach is probably more accurate, particularly for the LREEs due to the fact that late-stage interstitial silicate glasses (Fig. 4d–e), characterized by LREE enrichment, occur in many of these xenoliths. Fig. 8 shows the calculated melt compositions for a garnet-rich (DMP-440; 40% gt) and garnet-poor pyroxenite vein (DMP-124; 5% gt). The match between the

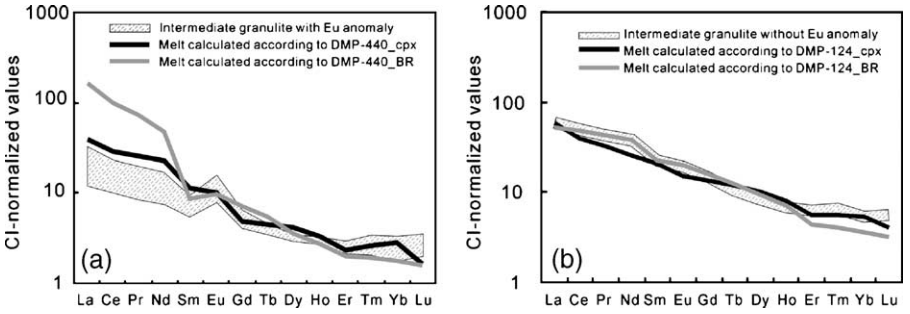

Fig. 8. CI-normalized REE patters of melts equilibrated with garnet pyroxenites. Melts were calculated according to bulk rock (BR) compositions of DMP-440 (0.4gt+0.40opx+0.1cpx+0.1ol), DMP-124 (0.50opx+0.3ol+0.15cpx+0.05gt) and singe grains of cpx, respectively. Parameters used for calculations are listed in Table 2.

calculated equilibrium REE abundance patterns and the intermediate–mafic granulites is remarkable.

These features indicate that the Type II garnet pyroxenites and granulites with SiO_2>50 wt.% have major and trace-element compositions consistent with equilibrium between the two. We thus argue that the Type II garnet pyroxenites in Hannuoba represent the products of reaction between a silicic melt and mantle peridotite and that the Mesozoic granulites may in fact represent these hybridized melts or evolved cumulates derived from such melts. If the garnet pyroxenites and the granulites could be demonstrated to be coeval, this would lend further support to the proposed link. Unfortunately, we have not yet found zircons in the garnet pyroxenites. If our interpretations are correct, the Type II garnet pyroxenites represent the first physical evidence for the hypothesized melt–rock reaction products necessary for generating evolved magmas with high Mg# from partial melts of mafic crust. In the next section, we discuss possible sources of this silicic melt and the implications of this process for continental crust formation.

5.3. Speculations on the origin of the silicic melts

If the Mesozoic granulites and the garnet pyroxenites are in fact linked and originate via melt–rock reaction between silicic melt and peridotite, this raises the question, where did the silicic melt come from? There was no active subduction zone in the Hannuoba region during the Mesozoic, so melting of subducting oceanic crust is not a viable option. Two possibilities for a silicic melt in the mantle are possible. The first is the generation of a silicic melt by fractional crystallization in a deep magma chamber. The second is delamination of dense, lower crustal mafic rocks into less dense, underlying mantle peridotite (e.g., [64–66]), followed by heating and generation of a silicic melt by partial melting of the descending, mafic crustal rocks [18,57,58]. The former seems unlikely for explaining the considerably radiogenic Sr isotopes of the (garnet-bearing) pyroxenites [45]. Furthermore, all granulite xenoliths undoubtedly have a crustal origin indicated by their unradiogenic Nd and radiogenic Sr isotopic compositions [41,44]. Thus, the delamination hypothesis seems more attractive. In such a process, foundering of ancient mafic crustal rock into the mantle peridotite would result in the mafic material being heated up and subsequently melted. This melt would be silicic and of low Mg# and evolved Nd–Sr isotopes, but as it rises up through the overlying mantle, its Mg# could increase due to reaction with the mantle. Such melts may continue to rise to form the protolith of the Mesozoic granulitic lower crust in Hannuoba.

One problem with the lower crustal delamination hypothesis is that it has previously been shown from Re–Os isotopic systematics on peridotite xenoliths from Hannuoba that much of the original Proterozoic and Archean lithospheric mantle was still intact at the time the Hannuoba basalts were erupted [30]. This suggests that either the lower crust did not delaminate or that, if it did, it delaminated through the lithospheric mantle. Given the high strength of lithospheric mantle, lower crustal delamination seems unlikely at face value. An alternative explanation would be

partial melting of basaltic layers that were previously subducted (*a fossil oceanic slab*) or underplated into the base of the lithospheric mantle. The type II garnet pyroxenites have considerably unradiogenic Sr isotopes ($^{87}Sr/^{86}Sr=0.7056–0.7068$) relative to their Nd isotopic compositions ($^{143}Nd/^{144}Nd=0.5130–0.5131$) (our unpublished data), which is a potential feature of ancient altered oceanic crust. Thus a fossil oceanic slab is preferred. Subsequent heating and/or delamination of such layers would not disturb the uppermost part of the lithospheric mantle.

Regardless of whether delamination occurred or not, the garnet pyroxenite and granulite data in Hannuoba are evidence for the reaction of silicic melts in the mantle. The high Mg#s of the Mesozoic Hannuoba granulites are interesting in light of the fact that compositional models of the bulk continental crust also appear to have high Mg# (although not as high as the Hannuoba granulites) [48]. It has been suggested that the high Mg# of average bulk continental crust is due to reaction of slab-derived melts with mantle peridotite [17] and that this process was most likely dominant in the Archean and Early Proterozoic when ambient mantle temperatures were high enough to melt subducting oceanic crust [10–13,16]. The Hannuoba garnet pyroxenites and granulites are evidence that similar processes can also occur during the Phanerozoic, albeit the ultimate origin of these Mesozoic silicic melts is probably not subducting oceanic crust, but possibly fossil oceanic slabs. What remains to be answered is how widespread this process is during the Phanerozoic.

6. Conclusions

The geological, mineralogical and geochemical evidence indicate that the Hannuoba garnet pyroxenite-bearing composite xenoliths represent products of melt–peridotite interactions. The high-Mg# intermediate–mafic granulite xenoliths could be derived from the melts involved in melt–peridotite interactions, and thus obtained its high-Mg# signature. The garnet pyroxenite-bearing composite xenoliths present physical evidence for the hypothesized melt–rock reaction products necessary for generating evolved magmas with high Mg# to build the high-Mg# andesitic signature of the continental crust.

Acknowledgements

We acknowledge the helpful comments by Peter Kelemen and Steve Shirey. We also thank R.L. Rudnick for review of an earlier draft of the manuscript and X.C. Wang for help in collecting xenoliths. This research is co-supported by the National Nature Science Foundation of China (grants 40133020 and 40373013), the Ministry of Science and Technology of China (grant 2003CB716501), the Program for Changjiang Scholars and Innovative Research Team in University (PCSIRT) and the Key Laboratory of Continental Dynamics, Northwest University.

References

[1] G.M. Yaxley, A.J. Crawford, D.H. Green, Evidence for carbonatitic metasomatism in spinel peridotite xenoliths from western Victoria, Australia, Earth Planet. Sci. Lett. 107 (1991) 305–317.

[2] D.A. Ionov, C. Dupuy, S.Y. O'Reilly, M.G. Kopylova, Y.S. Genshaft, Carbonated peridotite xenoliths from Spitsbergen: implications for trace element signature of mantle carbonate metasomatism, Earth Planet. Sci. Lett. 119 (1993) 283–297.

[3] P. Schiano, R. Clocchiatti, Worldwide occurrence of silica-rich melts in sub-continental and sub-oceanic mantle minerals, Nature 368 (1994) 621–624.

[4] P.K. Kepezhinskas, M.J. Defant, M.S. Drummond, Na-metasomatism in the island-arc mantle by slab melt–peridotite interaction: evidence from mantle xenoliths in the north Kamchatka arc, J. Petrol. 36 (1995) 1505–1527.

[5] P.K. Kepezhinskas, M.J. Defant, M.S. Drummond, Progressive enrichment of island arc mantle by melt–peridotite interaction inferred from Kamchatka xenoliths, Geochim. Cosmochim. Acta 60 (1996) 1217–1229.

[6] M.D. Norman, Melting and metasomatism in the continental lithosphere: laser ablation ICPMS analysis of minerals in spinel lherzolites from eastern Australia, Contrib. Mineral. Petrol. 130 (1998) 240–255.

[7] E. Wulff-Pedersen, E.R. Neumann, R. Vannucci, P. Bottazzi, L. Ottolini, Silicic melts produced by interaction between peridotite and infiltrating basaltic melts: ion probe data on glasses and minerals in veined xenoliths from La Palma, Canary Islands, Contrib. Mineral. Petrol. 137 (1999) 59–82.

[8] G. Prouteau, B. Scaillet, M. Pichavant, R. Maury, Evidence for mantle metasomatism by hydrous silicic melts derived from subducted oceanic crust, Nature 410 (2001) 197–200.

[9] J.L. Bodinier, M.A. Menzies, N. Shimizu, F.A. Frey, E. McPherson, Silicate, hydrous and carbonate metasomatism at Lherz, France: contemporaneous derivatives of silicate melt–harzburgite reaction, J. Petrol. 45 (2004) 299–320.

[10] R.H. Smithies, D.C. Champion, The Archaean high-Mg diorite suite: links to tonalite–trondbjemite–granodiorite magmatism and implications for early Archaean crustal growth, J. Petrol. 41 (1997) 1653–1671.
[11] H. Martin, Adakitic magmas: modem analogues of Archaean granitoids, Lithos 46 (1999) 41–429.
[12] S.B. Shirey, G.N. Hanson, Mantle-derived Archean monzodiorites and trachyandesites, Nature 310 (1984) 222–224.
[13] R.A. Stern, G.N. Hanson, Archean high-Mg granodiorite: a derivative of light rare earth element-enriched monzodiorite of mantle origin, J. Petrol. 32 (1991) 201–238.
[14] M.J. Defant, P. Kepezhinskas, Evidence suggests slab melting in arc magmas, EOS 82 (2001) 65–69.
[15] G.M. Yogodzinski, J.M. Lees, T.G. Churikova, F. Dorendorf, G. Woerner, O.N. Volynets, Geochemical evidence for the melting of subducting oceanic lithosphere at plate edges, Nature 409 (2001) 500–504.
[16] R.L. Rudnick, Making continental crust, Nature 378 (1995) 571–578.
[17] P.B. Kelemen, Genesis of high Mg# andesites and the continental crust, Contrib. Mineral. Petrol. 120 (1995) 1–19.
[18] P.B. Kelemen, K. Hanghoj, A.R. Greene, One view of the geochemistry of subduction-related magmatic arcs, with emphasis on primitive andesite and lower crust, in: R.L. Rudnick (Ed.), The Crust, Treatise on Geochemistry, vol. 3, Elsevier, 2003, pp. 593–659.
[19] R.P. Rapp, N. Shimizu, M.D. Norman, G.S. Applegate, Reaction between slab-derived melts and peridotite in the mantle wedge: experimental constraints at 3.8 GPa, Chem. Geol. 160 (1999) 335–356.
[20] M.G. Kopylova, S.Y. O'Reilly, Y.S. Genshaft, Thermal state of the lithosphere beneath Central Mongolia: evidence from deep-seated xenoliths from the Shavaryn-Saram volcanic centre in the Tariat depression, Hangai, Mongolia, Lithos 36 (1995) 243–255.
[21] M.G. Kopylova, J.K. Russell, H. Cookenboo, Petrology of peridotite and pyroxenite xenoliths from the Jericho kimberlite: implications for the thermal state of the mantle beneath the Slave craton, northern Canada, J. Petrol. 40 (1999) 79–104.
[22] K.D. Litasov, S.F. Foley, Y.D. Litasov, Magmatic modification and metasomatism of the subcontinental mantle beneath the Vitim volcanic field East Siberia: evidence from trace element data on pyroxenite and peridotite xenoliths from Miocene picrobasalt, Lithos 54 (2000) 83–114.
[23] D.G. Pearson, D. Canil, S.B. Shirey, Mantle samples included in volcanic rocks: xenoliths and diamonds, in: R.W. Carlson (Ed.), The Mantle and Core, Treatise on Geochemistry, vol. 2, Elsevier-Pergamon, Oxford, 2003, pp. 171–275.
[24] P.B. Kelemen, S.R. Hart, S. Bernstein, Silica enrichment in the continental upper mantle via melt/rock reaction, Earth Planet. Sci. Lett. 164 (1998) 387–406.
[25] D.Y. Liu, A.P. Nutman, W. Compston, J.S. Wu, Q.H. Shen, Remnants of >3800 Ma crust in the Chinese part of the Sino-Korean craton, Geology 20 (1992) 339–342.
[26] J.P. Zheng, W.L. Griffin, S.Y. O'Reilly, F.X. Lu, C.Y. Wang, M. Zhang, F.Z. Wang, H.M. Li, 3.6 Ga lower crust in central China: new evidence on the assembly of the North China craton, Geology 32 (2004) 229–232.
[27] G.C. Zhao, P.A. Cawood, S.A. Wilde, M. Sun, L.Z. Lu, Metamorphism of basement rocks in the Central Zone of the North China Craton: implications for Paleoproterozoic tectonic evolution, Precambrian Res. 103 (2000) 55–88.
[28] M.A. Menzies, W.M. Fan, M. Zhang, Paleozoic and Cenozoic lithoprobes and the loss of >120 km of Archean lithosphere, Sino-Korean craton, China, in: H.M. Prichard, T. Alabaster, N.B.W. Harris, C.R. Neary (Eds.), Magmatic Processes and Plate Tectonics, vol. 76, Geol Sot Spec Pub, London, 1993, pp. 71–81.
[29] W.L. Griffin, A. Zhang, S.Y. O'Reilly, C.G. Ryan, Phanerozoic evolution of the lithosphere beneath the Sino-Korean Craton, in: M. Flower, S.L. Chung, C.H. Lo, T.Y. Lee (Eds.), Mantle Dynamics and Plate Interactions in East Asia Geodynamics, vol. 27, American Geophysical Union, Washington, DC, 1998, pp. 107–126.
[30] S. Gao, R.L. Rudnick, R.W. Carlson, W.F. McDonough, Y.S. Liu, Re–Os evidence for replacement of ancient mantle lithosphere beneath the North China craton, Earth Planet. Sci. Lett. 198 (2002) 307–322.
[31] R.L. Rudnick, S. Gao, W.L. Ling, Y.S. Liu, W.F. McDonough, Petrology and geochemistry of spinel peridotite xenoliths from Hannuoba and Qixia, North China craton, Lithos 77 (2004) 609–637.
[32] F.Y. Wu, R.J. Walker, X.W. Ren, D.Y. Sun, X.H. Zhou, Osmium isotopic constraints on the age of lithospheric mantle beneath northeastern China, Chem. Geol. 196 (2003) 107–129.
[33] S. Gao, R.L. Rudnick, H.L. Yuan, X.M. Liu, Y.S. Liu, W.L. Xu, W.L. Ling, J. Ayers, X.C. Wang, Q.H. Wang, Recycling lower continental crust in the North China craton, Nature 432 (2004) 892–897.
[34] B.Q. Zhu, Theory and Applications of Isotope Systematics in Geosciences: Evolution of Continental Crust and Mantle in China, Science Press, Beijing, 1998 (in Chinese).
[35] Y. Song, F.A. Frey, Geochemistry of peridotite xenoliths in basalt from Hannuoba, eastern China: implications for subcontinental mantle heterogeneity, Geochim. Cosmochim. Acta 53 (1989) 97–113.
[36] M. Tatsumoto, A.R. Basu, W.K. Huang, J.K. Wang, G.H. Xie, Sr, Nd and Pb isotopes of ultramafic xenoliths in volcanic rocks of Eastern China: enriched components EMI and EMII in subcontinental lithosphere, Earth Planet. Sci. Lett. 113 (1992) 107–128.
[37] Q.C. Fan, R.X. Liu, H.M. Li, N. Li, J.L. Sui, Z.R. Lin, Zircon geochronology and rare earth element geochemistry of granulite xenoliths from Hannuoba (in Chinese), Chinese Sci. Bull. 43 (1998) 133–137.
[38] Q.C. Fan, J.L. Sui, R.X. Liu, X.M. Zhou, Eclogite facies garnet-pyroxenite xenoliths in Hannuoba area: new evidence of magma underplating (in Chinese with English Abs.), Acta Pet. Sin. 17 (2001) 1–6.
[39] S.H. Chen, S.Y. O'Reilly, X. Zhou, W.L. Griffin, G. Zhang, M. Sun, J. Feng, M. Zhang, Thermal and petrological structure of the lithosphere beneath Hannuoba, Sino-Korean Craton, China: evidence from xenoliths, Lithos 56 (2001) 267–301.

[40] G.H. Zhang, X.H. Zhou, S.H. Chen, M. Sun, Heterogeneity of the lower crust: evidence from geochemistry of the Hannuoba granulite xenoliths, Hebei province (in Chinese with English Abs.), Geochimica 27 (1998) 153–163.
[41] X.H. Zhou, M. Sun, G.H. Zhang, S.H. Chen, Continental crust and lithospheric mantle interaction beneath North China: isotopic evidence from granulite xenoliths in Hannuoba, Sino-Korean craton, Lithos 62 (2002) 111–124.
[42] Y.S. Liu, S. Gao, S.Y. Jin, S.H. Hu, M. Sun, Z.B. Zhao, J.L. Feng, Geochemistry and petrogenesis of lower crustal xenoliths from Hannuoba, North China: implications for the continental lower crustal composition and evolution at convergent margin, Geochim. Cosmochim. Acta 65 (15) (2001) 2589–2604.
[43] Y.S. Liu, S. Gao, X.M. Liu, X.M. Chen, W.L. Zhang, X.C. Wand, Thermodynamic evolution of lithosphere of the North China Craton: records from lower crust and upper mantle xenoliths from Hannuoba, Chin. Sci. Bull. 48 (2003) 2371–2377.
[44] Y.S. Liu, S. Gao, H.L. Yuan, L. Zhou, X.M. Liu, X.C. Wang, Z.C. Hu, L.S. Wang, U–Pb zircon dates and Nd, Sr and Pb isotopes of lower crustal xenoliths from North China Craton: insights on evolution of lower continental crust, Chem. Geol. 211 (2004) 87–109.
[45] Y.G. Xu, Evidence for crustal components in the mantle and constraints on crustal recycling mechanisms: pyroxenite xenoliths from Hannuoba, North China, Chem. Geol. 182 (2002) 301–322.
[46] S.A. Wilde, X.H. Zhou, A.A. Nemchin, M. Sun, Mesozoic crust–mantle interaction beneath the North China craton: a consequence of the dispersal of Gondwanaland and accretion of Asia, Geology 31 (2003) 817–820.
[47] S. Gao, X.M. Liu, H.L. Yuan, B. Hattendorf, D. Gunther, L. Chen, S.H. Hu, Determination of forty two major and trace elements in USGS and NIST SRM glasses by laser ablation-inductively coupled plasma-mass spectrometry, Geostand. Newsl. 26 (2002) 181–195.
[48] R.L. Rudnick, S. Gao, Composition of the Continental Crust, in: R.L. Rudnick (Ed.), The Crust, Treatise on Geochemistry, vol. 3, Elsevier, 2003, pp. 1–70.
[49] C.R. Stern, R. Kilian, Role of the subducted slab, mantle wedge and continental crust in the generation of adakites from the Andean Austral Volcanic Zone, Contrib. Mineral. Petrol. 123 (1996) 263–281.
[50] P. Kelemen, Assimilation of ultramafic rock in subduction-related magmatic arcs, J. Geol. 94 (1986) 829–843.
[51] G. Gaetani, T. Grove, The influence of water on melting of mantle peridotite, Contrib. Mineral. Petrol. 131 (1998) 323–346.
[52] K. Hirose, I. Kushiro, Partial melting of dry peridotites at high pressures: determination of compositions of melts segregated from peridotite using aggregates of diamond, Earth Planet. Sci. Lett. 114 (1993) 477–489.
[53] T. Kogiso, K. Hirose, E. Takahashi, Melting experiments on homogeneous mixtures of peridotite and basalt: application to the genesis of ocean island basalts, Earth Planet. Sci. Lett. 162 (1998) 45–61.
[54] L. Wasylenki, M. Baker, A. Kent, E. Stolper, Near-solidus melting of the shallow upper mantle: partial melting experiments on depleted peridotite, J. Petrol. 44 (2003) 1163–1191.
[55] R.P. Rapp, E.B. Watson, C.F. Miller, Partial melting of amphibolite/eclogite and the origin of Archean trondhjemites and tonalites, Precambrian Res. 51 (1991) 1–25.
[56] J. Arth, G. Hanson, Geochemistry and origin of early Precambrian crust of northwestern Minnesota, Geochim. Cosmochim. Acta 39 (1975) 325–362.
[57] L. Gromet, L. Silver, REE variations across the Peninsular Ranges batholith: implications for batholithic petrogenesis and crustal growth in magmatic arcs, J. Petrol. 28 (1987) 75–125.
[58] T. Zegers, P. van Keken, Middle Archean continent formation by crustal delamination, Geology 29 (2001) 1083–1086.
[59] G.M. Yogodzinski, R.W. Kay, O.N. Volynets, A.V. Koloskov, S.M. Kay, Magnesian andesite in the western Aleutian Komandorsky region: implications for slab melting and processes in the mantle wedge, GSA Bull. 107 (1995) 505–519.
[60] G. Shimoda, Y. Tatsumi, S. Nohda, K. Ishizaka, B.M. Jahn, Setouchi high-Mg andesites revisited: geochemical evidence for melting of subducting sediments, Earth Planet. Sci. Lett. 160 (1998) 479–492.
[61] K.L. Wang, S.L. Chung, C.H. Chen, C.H. Chen, Geochemical constraints on the petrogenesis of high-Mg basaltic andesites from the Northern Taiwan Volcanic Zone, Chem. Geol. 182 (2002) 513–528.
[62] C. Sen, T. Dunn, Dehydration melting of a basaltic composition amphibolite at 1.5 and 2.0 GPa: implications for the origin of adakites, Contrib. Mineral. Petrol. 117 (1994) 394–409.
[63] R.P. Rapp, E.B. Watson, Dehydration melting of metabasalt at 8–32 kbar: implications for continental growth and crust–mantle recycling, J. Petrol. 36 (1995) 891–931.
[64] R.W. Kay, S.M. Kay, Creation and destruction of lower continental crust, Geol. Rundsch. 80 (1991) 259–278.
[65] R.W. Kay, S.M. Kay, Delamination and delamination magmatism, Tectonophysics 219 (1993) 177–189.
[66] M. Jull, P. Kelemen, On the conditions for lower crustal convective instability, J. Geophys. Res. 106 (2001) 6423–6446.
[67] M. Klein, H.G. Stosch, H.A. Seck, N. Shimizu, Experimental partitioning of high field strength and rare earth elements between clinopyroxene and garnet in andesitic to tonalitic systems, Geochim. Cosmochim. Acta 64 (2000) 99–115.
[68] H. Fujimaki, M. Tatsumoto, K.I. Aoki, Partition coefficients of Hf, Zr, and REE between phenocrysts and groundmasses, J. Geophys. Res. 89 (1984) 662–672.
[69] Y.S. Liu, S. Gao, T.C. Luo, Geochemistry of terrain granulites from North China craton: implications for the composition of the lower continental crust (in Chinese, with English Abstr.), Geol. Geochem. 27 (1999) 40–46.
[70] S.R. Taylor, S.M. McLennan, The Continental Crust: Its Composition and Evolution, Blackwell, 1985.